

**2005 WJTA American Waterjet Conference
August 21-23, 2005 • Houston, Texas**

Paper 6A-2

PREDICTION OF A SINGLE IMPACT CRATER SHAPE IN AWJ MACHINING USING FEA

M. Junkar, B. Jurisevic, H. Orbanic
Laboratory for Alternative Technologies
University of Ljubljana
Ljubljana, Slovenia

M. Grah
Litostroj E.I.
Production of Power Generation and Industrial Equipment
Ljubljana, Slovenia

ABSTRACT

This contribution introduces a new approach to the Finite Element Analysis (FEA) method simulating the crater shape made by a single abrasive particle impact in Abrasive Water Jet (AWJ) machining. Impacts are observed at different impact angles and abrasive particle velocities. The proposed method is experimentally validated for stainless steel 1.4301 (AISI 304) as a workpiece material. Based on this experimental validation the simulation is extended to other engineering materials such as titanium alloy and aluminum alloy.

Organized and Sponsored by the Water Jet Technology Association

1 INTRODUCTION

There are many different attempts and approaches to simulate the AWJ cutting process. Some recent ones are briefly presented in the sequel. A phenomenological approach was used by Henning and Westkamper [1] to simulate the generated surface. Vikram and Ramesh Babu [2] combined the ballistic theory in order to predict the trajectory of the jet inside the workpiece material and Bitter's erosion theory to predict the workpiece material removal process. Hoogstrate et al. [3] developed a coherent set of models (material, kinematics, jet, process, process quantity and output quantity) for AJW cutting process simulation. A superposition of unit events represented by the interaction of a single abrasive particle with the workpiece material was applied by Lebar and Junkar [4] to predict the topology of the newly generated surface. An innovative approach using cellular automata was introduced by Orbanic and Junkar [5, 6], which is in comparison to the unit event based model computationally less demanding and gives similar results.

All those and many other models, which are not mentioned here, have a common point. They are designed to simulate the AWJ machining process as a whole, where the result is the generated surfaces on the workpiece after the interaction with the AWJ. In order to do that, the energy distribution (or a distribution of abrasive particles and their respective velocities) across the AWJ is taken as an input parameter for the simulations. Unfortunately, the structure of the AWJ and its energy distribution is not properly defined yet. Various authors used different energy distribution in their simulations as illustrated in Figure 1. It can be observed, that Henning and Westkamper [1] used a Gaussian bell distribution, while Lebar and Junkar [4] and Orbanic and Junkar [5] applied a uniform distribution to characterize the energy distribution across the jet in their simulation models. On the other hand, Chen and Siores [7] measured a double slope distribution using a Laser Doppler Anemometry (LDA). This is the main reason why in the presented modeling attempt only single abrasive particle impacts are simulated instead of making a superposition of the craters in order to simulate the generated surface after AWJ cutting.

Beside the simulation models based on various principles, the AWJ process was modeled and simulated by using the Finite Element Analysis (FEA) approach. In this domain Guo et al. [8] simulate the AWJ drilling process with an implicit FEA method. They validated the model by observing the stress field generated by the static load of the jet in the sample using a moiré interferometry technique. On the other hand, Hassan and Kosmol [9] applied an implicit FEA method to simulate the erosion on the workpiece produced by a single abrasive particle. Mohan and Kovacevic [10] simulated the crack propagation in a Portland Cement Concrete (PCC) slab slotted by an AWJ.

After the exposure of the objectives and approaches used for this investigation the applied FEA method is described. It follows a description of the experimental validation, which was executed on stainless steel 1.4301 (AISI 304). The proposed method was further implemented to simulate the crater shapes made at different impact angles on materials such as titanium alloy Ti-6Al-2Sn-4Zr-2Mo, aluminum alloy AlMg1SiCu (6061-T6) and nickel-based superalloy (Waspaloy). At the end the conclusions are traced with an insight into future work in the field.

2 OBJECTIVES AND APPROACHES

In this investigation an improved FEA method is used to predict the crater shape (S_C) produced after a single abrasive particle impact in different workpiece materials such as titanium alloy Ti-6Al-2Sn-4Zr-2Mo, aluminum alloy AlMg1SiCu (6061-T6) and nickel-based superalloy designated as Waspaloy. The main FEA code was previously experimentally validated on stainless steel 1.4301 (AISI 304), of which a detailed description is available [12]. This procedure is graphically illustrated in Figure 2. In the sequel, the applied FEA method is briefly presented and the corresponding experimental validation of it is described. In chapter 5 the simulation results for titanium alloy Ti-6Al-2Sn-4Zr-2Mo, aluminum alloy AlMg1SiCu (6061-T6) and nickel-based superalloy are presented in cases for impacts at 90, 60 and 30 degrees. At the end conclusions are collected with an insight of future activities in the field.

In Abrasive Water Jet (AWJ) cutting the workpiece material is removed mainly due to high-velocity impacts of hard abrasive particles. During AWJ cutting, the interface between the tool and the workpiece is a curved cutting front. The curvature of the cutting front depends on many process parameters, but mainly on the traverse rate of the cutting head. However, it can be observed, that the abrasive particles impact the workpiece material on the cutting front at angles (α_1) from almost 0 degrees at the top of the cut and up to 90 degrees at the bottom of the cut, especially when the cut does not go through all the sample thickness (T_S). Additionally, since the cutting step mechanism takes place during the process, which was reported by Hashish [11] it is reasonable to assume that many abrasive particles impacts take place at 90 degrees even when the cut goes through all the workpiece thickness. A model of such a cutting front with a cutting step, where various impact angles are illustrated is presented in Figure 3.

3 APPLIED FEA METHOD

For the numerical simulation an explicit FEA method is applied. Comparing to other attempts of simulating the AWJ process with the FEA, some improvements are implemented in the presented method. The material model is based on the true stress - true strain curve as an elasto-plastic material and it takes into account the hardening of the material due to plastic deformations. Additionally, dynamic properties such as velocity and gravity were considered. The abrasive particles are taken as rigid spherical objects with a predefined mass and initial velocity, which is the same as the velocity of abrasive particles after the acceleration process. Other abrasive parameters relevant for the numerical simulation are listed in Table 1.

In modeling the single abrasive particle impact in AWJ machining, high-speed of the abrasive particle (v_A) up to few 100 m/s, small dimension of the particle (d_A) in range of some 100 μm and the fact that the impact takes place in a very short time represents important issues, which inevitably lead to a numerical stability problem. Due to contact problems between the abrasive particle and the workpiece material, and because of the small duration of the impact, an implicit numerical code couldn't be applied. According to that, ANSYS/LS-DYNA was chosen, since it is an explicit numerical program, designed to solve different types of impacts.

Because the impact time of an abrasive particle is in the range of few μs , the critical time interval in the simulation plays a crucial role in FEA simulation. This critical time interval is used by

ANSYS/LS-DYNA to verify if a contact was established between the abrasive particle and the workpiece material. In the case when the critical time is too long, it can occur that no impact is perceived in the simulation. On the other hand, when the critical time interval is too short, the simulation would take too much time to be practically useful. These facts reveal the crucial importance of defining an appropriate set of units.

The critical time is derived from length and mass units. The selected set of units has to fulfill the condition that the critical time interval is much smaller than the time in which the impact takes place [12]. When this condition is fulfilled, the impact of an abrasive particle on the workpiece surface will be detected and properly simulated.

For fast numerical modeling a program in Python (GPL license) was developed, which creates a text-based file. This file contains APDL (ANSYS Parametric Design Language) orders, which instructs ANSYS/LS-DYNA how to build and solve the numerical model. As starting conditions, the initial velocity and also gravity are imposed to the abrasive particle.

During the FEA simulation in ANSYS/LS-DYNA, it is verified, after each time interval if the contact between the abrasive particle and the workpiece surface takes place. The selected type of the contact has to fulfill two conditions. In the first place, the contact has to be a surface to surface type. Besides that, the contact type has to allow a surface to experience material failure during the contact. Both demands are fulfilled in case, where an Eroding Surface To Surface (ESTS) type of contact is chosen [12].

The selected type of contact correctly models a possible punch in the workpiece material, because numerical instabilities can arise if a different type of contact is chosen. In this way, the local fracture of workpiece material was correctly modeled. The abrasive particle was modeled using rigid 3D solid (tetrahedral) elements. The workpiece material was modeled with 3D solid (brick) elements with an elastic-plastic material model. A Piecewise Linear Plasticity material model was applied, which is very appropriate for steel and other metals.

4 EXPERIMENTAL VALIDATION OF THE PROPOSED FEA METHOD ON STAINLESS STEEL 1.4301 (AISI 304)

The applied FEA method has been recently experimentally validated for stainless steel 1.4301 (AISI 304) as a workpiece material [12]. The relevant material properties are listed in Table 2. All the samples were ground prior to the experiment and the average surface roughness $R_a=0.83 \mu\text{m}$ was achieved. Craters shape after impacts at different impact angles and water pressures are observed and compared with the simulated ones at different impact angles and abrasive particles velocities. As described before, the impacts are numerically simulated at different impact angles of abrasive particles and its velocities. In the experimental validation the samples were exposed to the jet at different impact angles using a specially developed workpiece holder, which allows us to expose the workpiece surface at impact angles between 0 and 90 degrees. On the other hand it is extremely difficult to define the actual velocity of abrasive particles. The only practical way to do this is to find a relation between the water pressure (p_w) and the abrasive particles velocity. For injection AWJ systems it is known that the abrasive particles velocity depends on the velocity of the Water Jet (WJ), which accelerates the abrasive particles in the cutting head.

Additionally, the final velocity of an abrasive particle depends on the ratio between the water mass flow and abrasive mass flow and of course on the geometry of the cutting head itself. In this investigation it is assumed that the initial WJ velocity is proportional to the square root of the water pressure as defined by Equation 1.

$$v_{w,0} \approx \sqrt{\frac{2 \cdot p_w}{\rho_w}} \quad (1)$$

During the acceleration process the momentum is transferred from the WJ to the abrasive particles. Beside water and abrasive particles, a flow of air is present in the acceleration process. In this case the momentum transfer is described by Equation 2.

$$m_A \cdot v_{A,0} + m_W \cdot v_{W,0} + m_{air} \cdot v_{air,0} = m_A \cdot v_{A,1} + m_W \cdot v_{W,1} + m_{air} \cdot v_{air,1} \quad (2)$$

In Equation 2, m_A , m_W and m_{air} are the abrasive, water and air mass flow, respectively; $v_{A,0}$, $v_{W,0}$ and $v_{air,0}$ are the initial velocities of the abrasive, water and air, respectively; $v_{A,1}$, $v_{W,1}$ and $v_{air,1}$ are the final velocities after the acceleration process of the abrasive, water and air, respectively. From experience, the following assumptions can be made: the initial velocity of abrasive particles and air can be neglected, since they are much smaller than the initial velocity of water ($v_{A,0} \ll v_{W,0}$, $v_{air,0} \ll v_{W,0} \Rightarrow v_{A,0} \approx 0$, $v_{air,0} \approx 0$). The other parameter that can be neglected in Equation 2 is the mass flow of air, since it represents only about 2% of the total jet mass ($m_{air} \ll m_A$, $m_W \ll m_A \Rightarrow m_{air} \approx 0$). Taking into account all those assumption, the impact velocity of abrasive particles can be estimated with Equation 3.

$$v_{A,1} = \frac{m_W \cdot (v_{W,0} - v_{W,1})}{m_A} \quad (3)$$

In order to calculate the final velocity of abrasive particles the final velocity of the water has to be known, which is not the case in AWJ machining. Nevertheless, from Equation 1 and Equation 3, a relation between the water pressure and final velocity of the abrasive particles can be approximated as shown in Equation 4.

$$v_{A,1} \approx C_1 \cdot \sqrt{p_w} + C_2 \quad (4)$$

The parameters C_1 and C_2 describe the acceleration process and they depend on various process parameters such as the abrasive properties, geometry of the cutting head components, etc. However, Equation 4 shows how the final velocity of the abrasive particles is proportional to the square root of the water pressure, what is a crucial information for the experimental validation of the proposed FEA method. Taking all this into account the velocity of abrasive particles for the numerical simulation and the respective water pressures used in the experimental validation were selected as listed in Table 3, where a total of nine different parameter setups are defined.

During the experimental validation a shallow trace was engraved using high traverse rate (v_T) of the cutting head in order to observe the shape of single, isolated craters on the sample surface as

shown in Figure 2. All the experiments were performed on a OMAX type 2652A/20HP cutting system, with a Böhler cutting head. The high-pressure water was supplied from a hydraulic intensifier (Böhler Ecotron 403). The abrasive material was Garnet #80, of which more details are collected in Table 4.

The minor (d_1) and major (d_2) dimensions of the craters were measured using a freeware image processing software Image Tool. Crater pictures were acquired with a digital camera JVC TK-870E, which was placed on a microscope Leitz Ortoplan with optical magnification 50:1. All further data analysis including the graphical presentation of results were carried out in MatLab where the sphericity of the craters (S_C) was defined according to Equation 5.

$$S_C = \frac{d_1}{d_2} \quad (5)$$

In this experimental validation $N_C=200$ craters were observed for each scenario what gives a total of 1800 measured craters through all the validation. The experimental results in terms of crater sphericity for all three different water pressures and impact angles are collected in Figure 4 and the comparison between the FEA simulations and experimental validation in Figure 5. The results of the experimental validation are also collected in Table 5, in which the relative difference (Δ_S) between the FEA simulation and experimental validation is calculated.

From the results collected in Figure 5 and Table 5 it can be observed, that the simulated craters are more spherical than the measured one. This can be explained by the fact that in the FEA simulations the abrasive particles are modeled as perfect spherical bodies, while the measured sphericity of the abrasive material used for the experimental validation is about 0.6884. This difference between the modeled and actual abrasive particles sphericity causes a drift between the simulation and the experiment.

5 APPLICATION OF THE PROPOSED FEA METHOD TO OTHER ENGINEERING MATERIALS

After the successful experimental validation on stainless steel 1.4301 (AISI 304), the proposed FEA method was applied to simulate and predict the shape of single craters produced at different impact angles of abrasive particles. After the preliminary investigation [12] it was decided, that only the influence of the impact angle will be observed in this case. In all simulations the impact velocity of abrasive particles was always set at 200 m/s.

For the prediction of crater shapes at different impact angles the same FEA code was used as described in the previous sections. The only difference was in the new workpiece material models, of which the data are collected in Table 5.

5.1 Titanium alloy Ti-6Al-2Sn-4Zr-2Mo

This alloy was developed for improved elevated temperature performance. The base is formed of titanium and aluminum, while the overall performance is enhanced by various additions. The strength at both, room and elevated temperatures, the creep and thermal stability are improved by

molybdenum. Addition of tin and zirconium contribute to higher strength. A small addition of silicon (about 0.08%) substantially increases the creep strength. This combination results in a creep resistant and relatively stable alloy at high temperatures up to 565°C (1050°F). This material is used for advanced performance gas turbine engine application.

5.2 Aluminum alloy AlMg1SiCu (6061-T6)

The 6061 series aluminum alloy is used in a wide range of applications, including cryogenic application where high toughness is required. This material has an excellent joining characteristics, good acceptance of applied coatings and its combines relatively high strength, corrosion resistance and is widely available. A wide range of applications comprises aircraft fittings, camera lens mounts, couplings, marine fittings and hardware, electrical fittings and connectors, magneto parts, brake and hydraulic pistons, appliance fittings, valves, etc.

5.3 Nickel-based superalloy Waspaloy

Waspaloy is an age hardenable superalloy with excellent strength at temperature up to about 980°C (1800°F). Due to its high performance at elevated temperature this alloy is widely used for gas turbine and aerospace components. However, it is also very difficult to machine with conventional cutting processes such as milling and turning, what makes it a perfect candidate for AWJ machining.

5.4 FEA simulations results

The FEA simulation results for all the material described above are presented in diagrams in Figure 6-8. Additionally, pictures of the craters are corresponding the respective points in the diagrams. From these diagrams it can be observed that the impact angle of abrasive particles has the strongest influence on the crater shape in case when the target material is AlMg1SiCu, while on the other hand the smallest influence was encountered in case of the nickel based superalloy (Waspaloy). According to these FEA results, the most stable material during AWJ machining should be Waspaloy, while in case of AlMg1SiCu the machining quality depends on the impact angles of abrasive particles during the process.

However, all these numerical results are not experimentally validated since the implemented FEA method was validated in case of stainless steel 1.4301 (AISI 304) and the simulation was extended to metals, with similar elasto-plastic behavior.

6 CONCLUSION

In this paper an explicit FEA method is presented, which allows us to simulate the crater shapes after produced by a single abrasive particle impact at different impact angles. The proposed method was experimentally validated for the case when the workpiece material is stainless steel 1.4301 (AISI 304) [12]. The main objective of this investigation was the extrapolation of the method on other engineering materials such as titanium alloy Ti-6Al-2Sn-4Zr-2Mo, aluminum alloy AlMg1SiCu (6061-T6) and nickel-based superalloy (Waspaloy). All these materials exhibit the same elasto-plastic behavior like stainless steel 1.4301, on which the FEA method was

experimentally validated. In order to simulate the crater shapes on different workpiece materials the material model, which is mainly based on the true stress - true strain curve has to be available.

This work is just a part of a widely defined investigation, extended to research other mechanisms involved in the AWJ machining process. An interesting effect would be the influence of the abrasive particle size, especially from the perspective of applying AWJ machining to micro manufacturing. Beside that, the proposed method will be applied to analyze if there is any relevant rotation of abrasive particles at the impact of the workpiece material.

7 ACKNOWLEDGEMENT

This work is supported by the "Multi-Material Micro Manufacture: Technology and Applications (4M)" Network of Excellence, Contract Number NMP2-CT-2004-500274 and by the "Virtual Research Lab for a Knowledge Community in Production (VRL-KCiP)" Network of Excellence, Contract Number NMP2-CT-2004-507487, both within the EU 6th Framework Program. The authors would also like to express their gratitude to the Slovene Ministry of Higher Education, Science and Technology.

8 REFERENCES

- [1] Henning, A., Westkamper, E.: "Modelling of wear mechanisms at the abrasive waterjet cutting front." In: Summers DA, editor. Proceedings of the 2003 WJTA American Waterjet Conference, Houston (Texas, USA): WJTA, paper 3-A, 2003.
- [2] Vikram, G., Ramesh Babu, N.: "Modelling and analysis of abrasive water jet cut surface topography" *Int J Machine Tools and Manuf.*; Vol. 42, pages 1345-1354, 2002.
- [3] Hoogstrate, A., M., Karpuschewski., B., van Luttervelt, C., A., Kals, H., J., J.: "Modeling of High Velocity, Loose Abrasive Machining Processes" *Annals of the CIRP*; 51(1): 263-266, 2002.
- [4] Lebar, A., Junkar, M.: "Simulation of abrasive water jet cutting process: Part1. Unit event approach." *Modelling Simul. Mater. Sci. Eng.*, Vol.12, No. 6, pp. 1159-1170, 2004.
- [5] Orbanic, H., Junkar, M.: "Simulation of abrasive water jet cutting process: Part2. Cellular automata approach" *Modelling Simul. Mater. Sci. Eng.*, Vol. 12, No. 6, pages 1171-1184, 2004.
- [6] Orbanic, H., Junkar, M.: "Cellular automata in mechanical engineering" In: Junkar M, Levy PR, editors. Proceedings of the 6th International Conference on Management of Innovative Technologies, Piran (Slovenia), LAT, TAVO, pp. 139-147, 2003.
- [7] Chen, F., L., Siores, E.: "The effect of cutting jet variation on surface striation formation in abrasive water jet cutting" *J Mat Proc Tech.*, Vol. 135: pages 1-5, 2003.
- [8] Guo, Z., Ramulu, M., Jenkins, M., G.: "Analysis of the waterjet contact/impact on target material" *Optics and Lasers in Engn.*, Vol 33, pages 121-139, 2000.
- [9] Hassan, A., I., Kosmol, J.: "Finite element modeling of abrasive water-jet machining (AWJM)" In Ciccù R, editor. 15th International Conference on Jetting Technology, Ronneby (Sweden): BHR Group Limited, pp. 321-333, 2000.

- [10] Mohan, R., S., Kovacevic, R.: "Finite element modeling of crack propagation in PCC slabs slotted with abrasive water jet". In: Hashish M, editor. Proceedings of the 10th American Waterjet Conference, Houston (Texas, USA): WJTA, paper 5, 1999.
- [11] Hashish, M.: "Visualization of the Abrasive-Waterjet Cutting Process." *Experimental Mechanics*, 28: 159-169, 1988.
- [12] Junkar, M., Jurisevic, B., Fajdiga, M., Grah, M.: "Finite element analysis of single-particle impact in abrasive water jet machining" *International Journal of Impact Engineering*, November 2004 - *available online*.

9 NOMENCLATURE

Symbols:

| | | | |
|------------|--|--------------|--|
| $\#_A$ | abrasive mesh number [-] | $R_{p\ 0.2}$ | yield stress [MPa] |
| A_M | elongation [%] | S_C | crater sphericity [-] |
| C_1, C_2 | constants describing the abrasive acceleration process [-] | $S_{C,exp}$ | measured crater sphericity [-] |
| d_1 | minor crater dimension [μm] | $S_{C,FEA}$ | simulated crater sphericity [-] |
| d_2 | major crater dimension [μm] | $S_{C,FEA}$ | simulated crater sphericity [-] |
| d_A | diameter of abrasive particles [μm] | T_S | sample thickness [mm] |
| d_F | diameter of the focusing tube [mm] | v_A | abrasive particle velocity [m/s] |
| d_O | diameter of the orifice [mm] | $v_{A,0}$ | initial velocity of abrasive before the acceleration process [m/s] |
| E_A | elastic module of abrasive [MPa] | $v_{A,1}$ | final velocity of abrasive at the exit from the cutting head [m/s] |
| E_{AWJ} | AWJ kinetic energy [J] | $v_{air,0}$ | initial velocity of air before the acceleration process [m/s] |
| E_M | elastic module of the workpiece material [MPa] | $v_{air,1}$ | final velocity of air at the exit from the cutting head [m/s] |
| h_{SO} | stand-off distance [mm] | v_T | traverse rate of the cutting head [mm/s] |
| l_F | length of the focusing tube [mm] | $v_{W,0}$ | initial velocity of water before the acceleration process [m/s] |
| m_A | abrasive mass flow [g/min] | $v_{W,1}$ | final velocity of water at the exit from the cutting head [m/s] |
| m_W | water mass flow [g/min] | | |
| N_C | number of measured craters [-] | | |
| p_W | water pressure [MPa] | | |
| R_a | average surface roughness [μm] | | |
| r_{AWJ} | AWJ radius [mm] | | |
| R_m | tensile strength [MPa] | | |

Greek letters:

| | | | |
|------------|--|----------|---|
| α_I | impact angle [$^\circ$] | ρ | specific material density [kg/m^3] |
| Δ_S | relative difference between simulated and measured crater sphericity [%] | ρ_A | abrasive density [kg/m^3] |
| ν_A | Poisson coefficient for abrasive [-] | ρ_M | density of the workpiece material [kg/m^3] |
| ν_M | Poisson coefficient of the workpiece material [-] | ρ_W | water density [kg/m^3] |

10 TABLES

Table 1. Abrasive properties used in the FEA simulation

| | |
|---------------------------------|------------------------|
| particles shape | spherical |
| elastic module (E_A) | 2.48×10^5 MPa |
| Poisson coefficient (ν_A) | 0.27 |
| abrasive density (ρ_A) | 4000 kg/m ³ |
| particle diameter (d_A) | 100 μ m |

Table 2. Material properties for stainless steel 1.4301 (AISI 304)

| | |
|---------------------------------|------------------------|
| material density (ρ_M) | 8030 kg/m ³ |
| elastic module (E_M) | 1.95×10^5 MPa |
| Poisson coefficient (ν_M) | 0.27 |
| yield stress ($R_{p0.2}$) | 316 MPa |
| tensile strength (R_m) | 623 MPa |
| elongation (A_M) | 55 % |

Table 3. Variable parameters in the FEA simulation and experimental validation for stainless steel 1.4301 (AISI 304)

| FEA simulation | | experimental validation | |
|------------------|--|-------------------------|----------------------|
| impact angle [°] | impact velocity of abrasive particle [m/s] | impact angle [°] | water pressure [MPa] |
| 30 | 180 | 30 | 200 |
| 60 | | 60 | |
| 90 | | 90 | |
| 30 | 200 | 30 | 250 |
| 60 | | 60 | |
| 90 | | 90 | |
| 30 | 220 | 30 | 300 |
| 60 | | 60 | |
| 90 | | 90 | |

Table 4. Properties of the abrasive material used in the experimental validation

| | |
|---------------------------------|----------------------------------|
| type of abrasive | Garnet |
| abrasive mesh ($\#_A$) | 80 |
| average particle size (d_A) | 190 μ m |
| abrasive density (ρ_A) | ≈ 4000 kg/m ³ |
| abrasive hardness | 8÷9 Mohs scale |

Table 5. Comparison of FEA simulation and experimental results for stainless steel 1.4301 [12]

| impact angle α_I [°] | 30 | 60 | 90 |
|---------------------------------------|-------------|-------------|-------------|
| measured sphericity at $p_W=200$ MPa | 2.2100 | 1.6573 | 1.3166 |
| simulated sphericity at $v_A=180$ m/s | 1.3280 | 1.1040 | 1.0000 |
| relative difference, Δ_S [%] | 39.9 | 33.4 | 31.7 |
| measured sphericity at $p_W=250$ MPa | 2.0066 | 1.6027 | 1.2605 |
| simulated sphericity at $v_A=200$ m/s | 1.3370 | 1.1040 | 1.0000 |
| relative difference, Δ_S [%] | 33.4 | 31.1 | 26.1 |
| measured sphericity at $p_W=300$ MPa | 2.0319 | 1.5686 | 1.2115 |
| simulated sphericity at $v_A=220$ m/s | 1.4183 | 1.0820 | 1.0000 |
| relative difference, Δ_S [%] | 30.2 | 31.0 | 21.2 |

Table 6. Material properties used in the FEA simulation of titanium alloy Ti-6Al-2Sn-4Zr-2Mo, aluminum alloy AlMg1SiCu (6061-T6) and Nickel-based superalloy Waspaloy

| material | Ti-6Al-2Sn-4Zr-2Mo | AlMg1SiCu | Waspaloy |
|--|--------------------|-----------|----------|
| material density (ρ_M) [kg/m ³] | 4539.52 | 2712.64 | 8248.64 |
| elastic module (E_M) [MPa] | 113765 | 68948 | 210980 |
| Poisson coefficient (ν_M) [-] | 0.32 | 0.33 | 0.3 |
| yield stress ($R_{p0.2}$) [MPa] | 221 | 104 | 442 |
| tensile strength (R_m) [MPa] | 992 | 138 | 1003 |
| elongation (A_M) [%] | 10 | 10 | 20 |

11 FIGURES

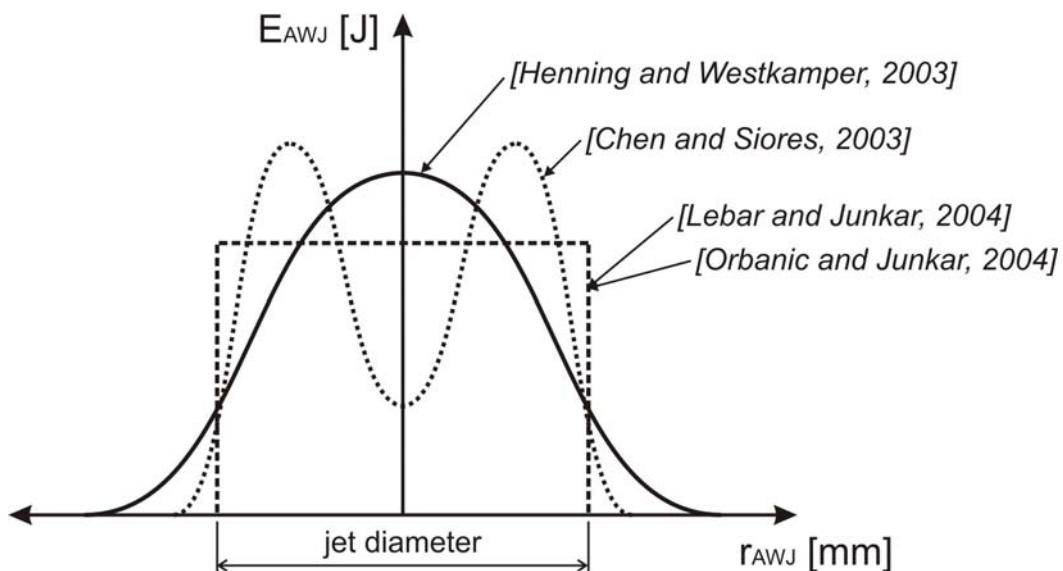
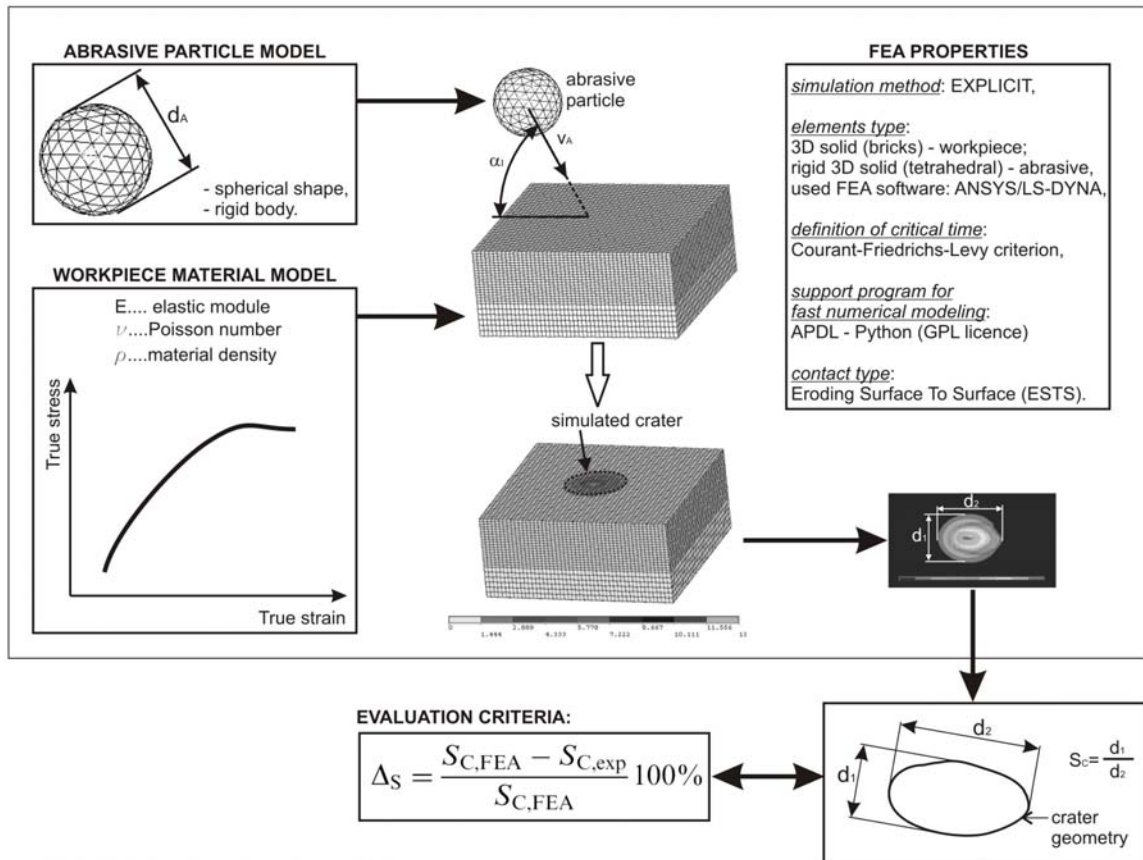


Figure 1. Different types of energy distribution profiles in the AWJ.

FEA SIMULATION



EXPERIMENTAL VALIDATION

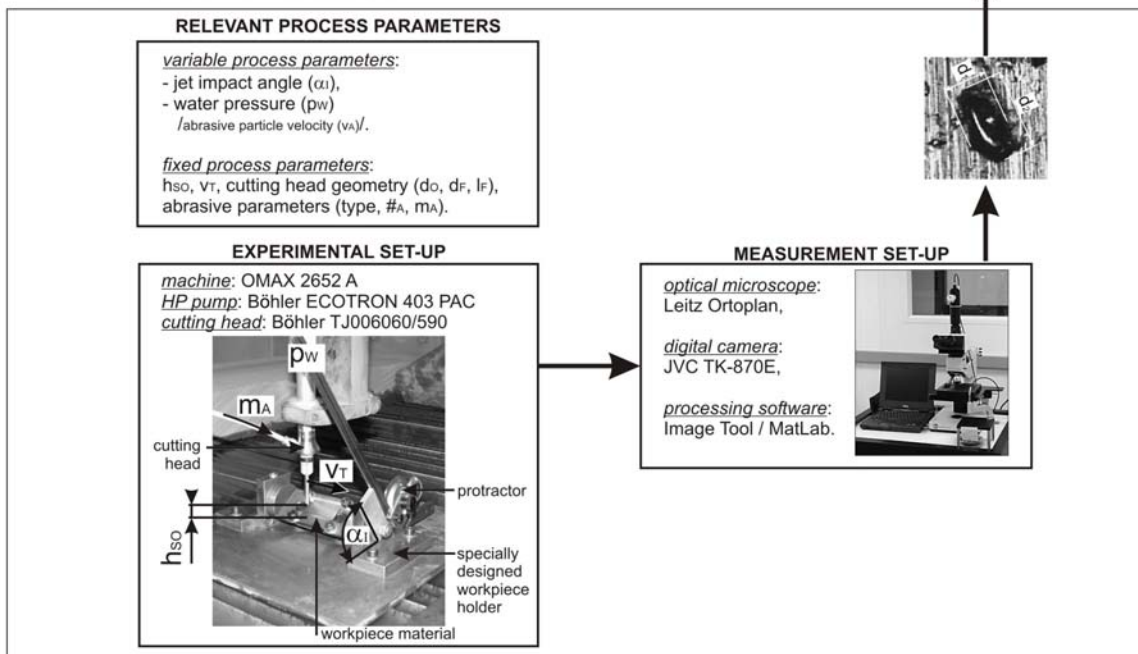


Figure 2. Proposed approach of FEA simulation and experimental validation

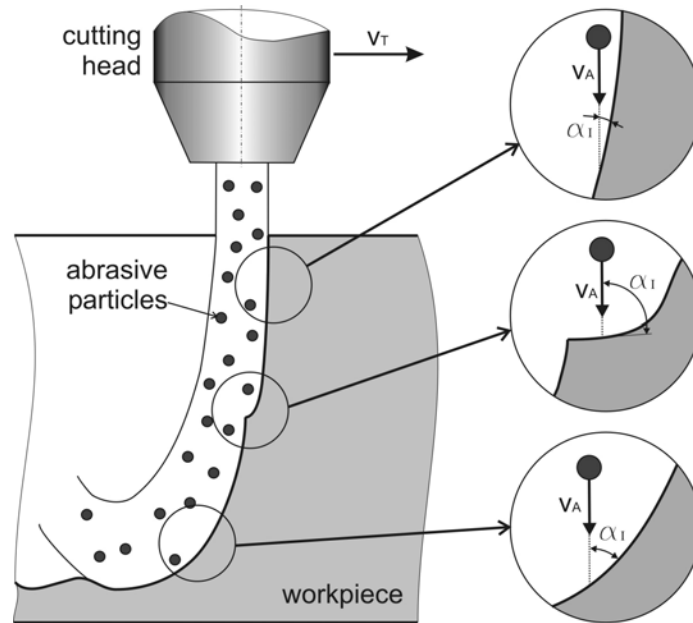


Figure 3. Shape of a cutting front in AWJ cutting and impact angles of abrasive particles.

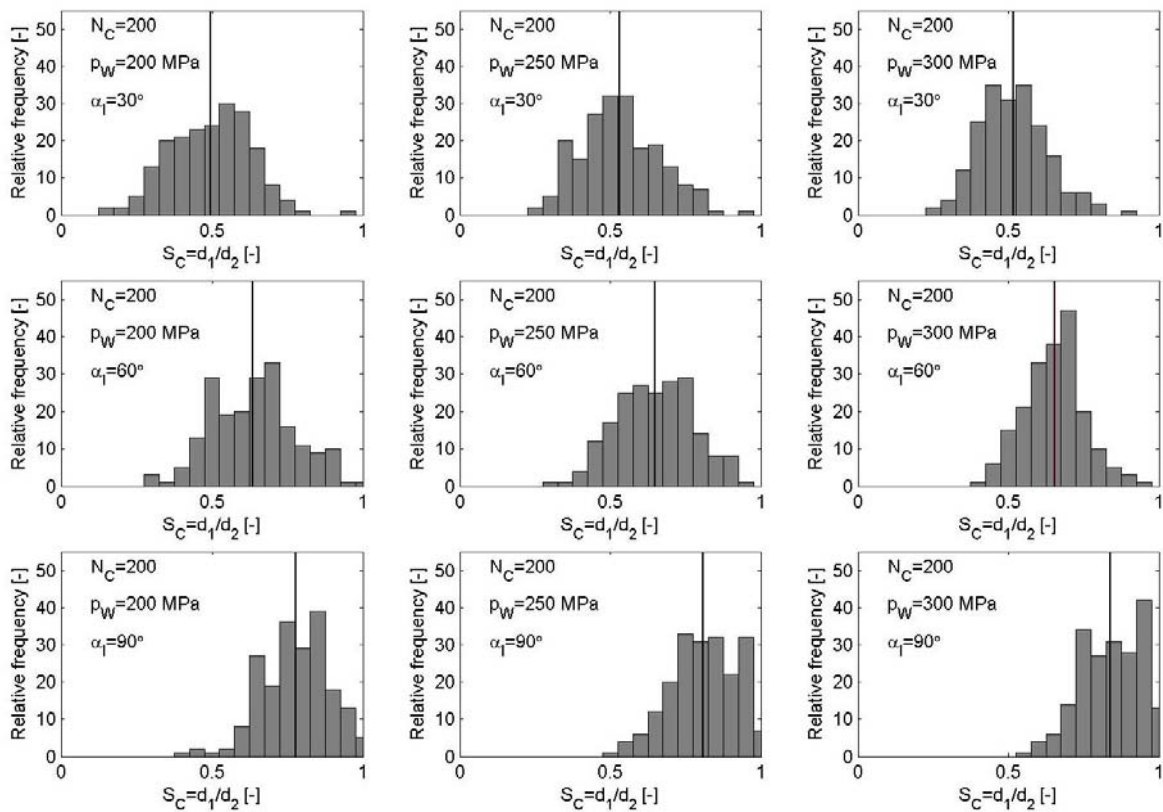


Figure 4. Measured craters sphericity in the experimental validation [11]

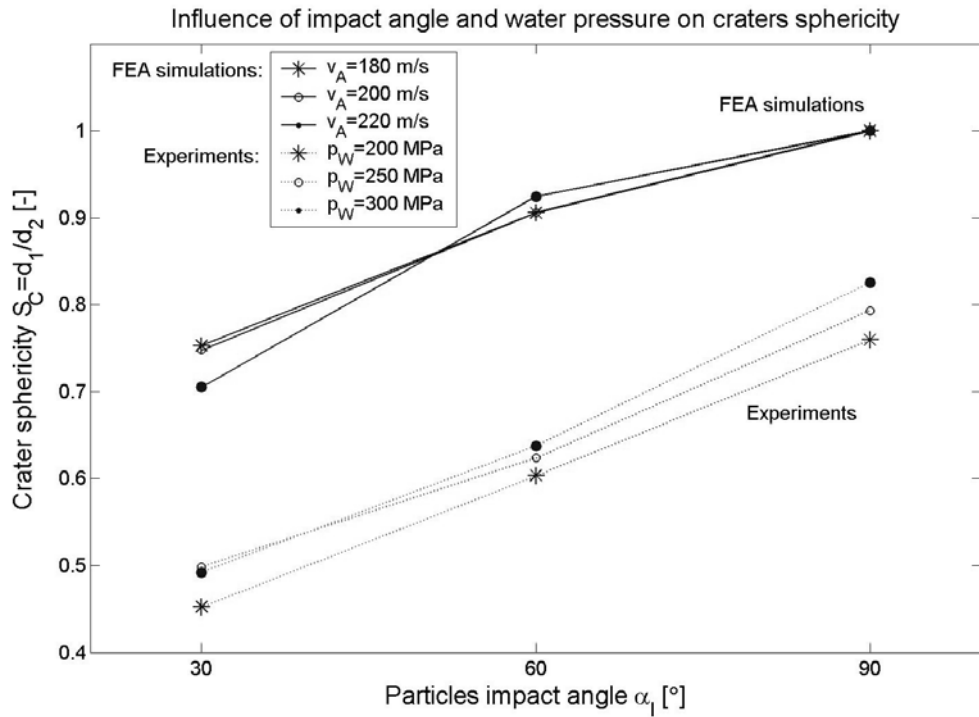


Figure 5. Numerical and experimental results in case of stainless steel 1.4301 (AISI 304) [12]

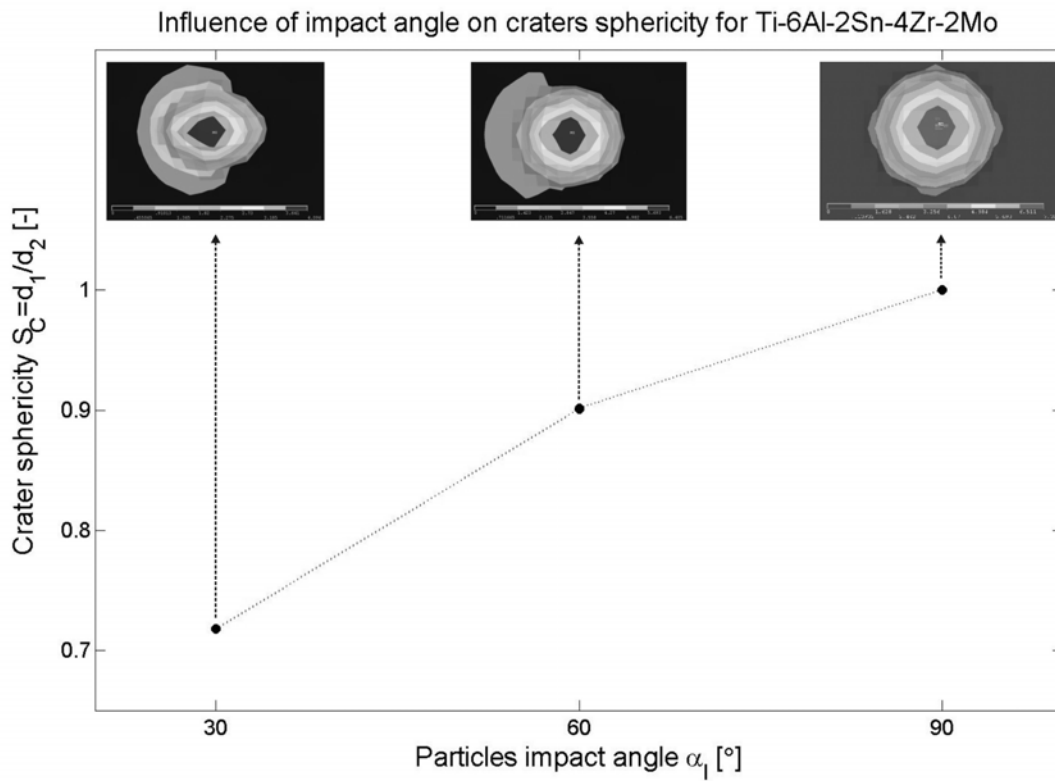


Figure 6. FEA results in case of Ti-6Al-2Sn-4Zr-2Mo

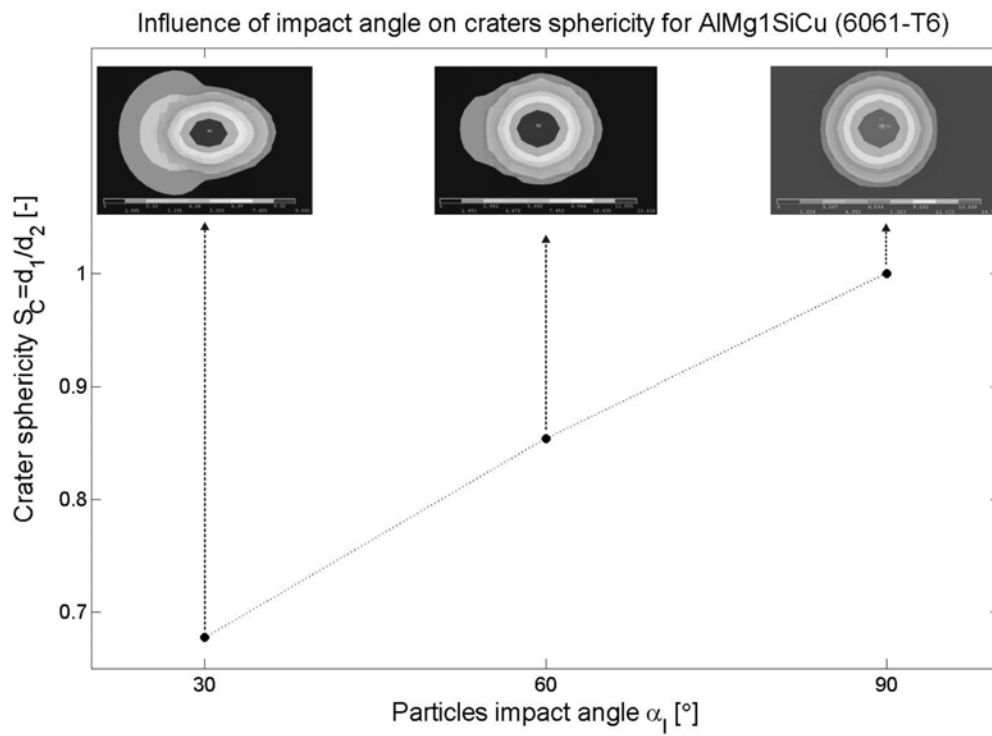


Figure 7. FEA results in case of AlMg1SiCu (6061-T6)

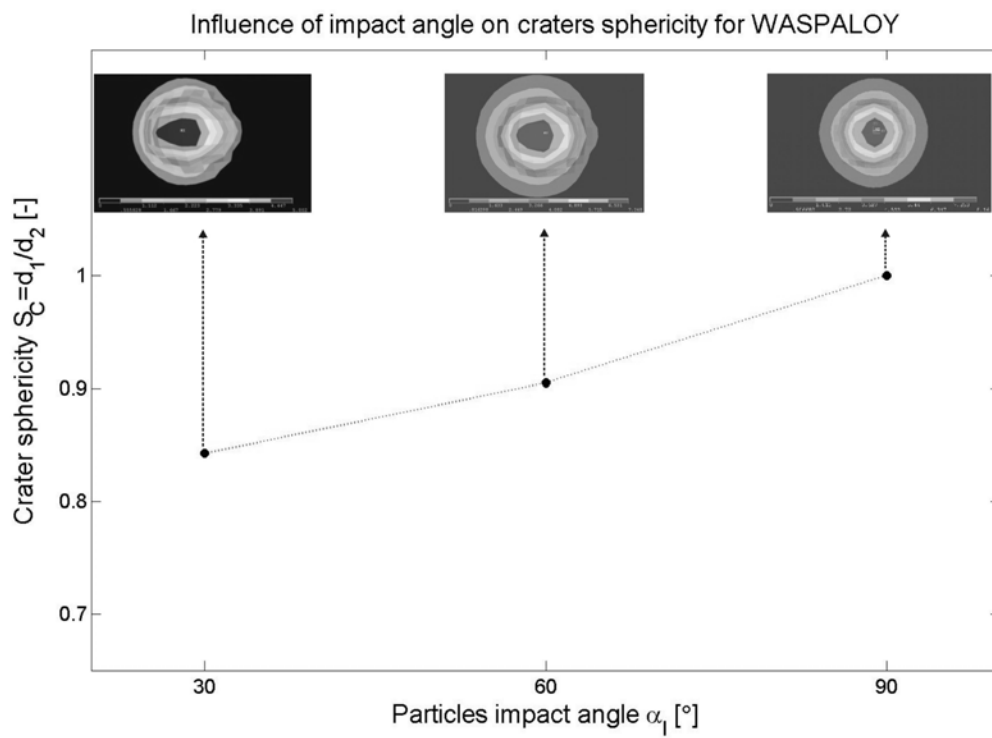


Figure 8. FEA results in case of nickel based superalloy Waspaloy